Voltage-controlled superconducting quantum bus

L. Casparis,[1] N. J. Pearson,[1,2] A. Kringhøj,[1] T. W. Larsen,[1] F. Kuemmeth,[1] J. Nygård,[1,3] P. Krogstrup,[1] K. D. Petersson,[1] and C. M. Marcus[1]

[1]*Center for Quantum Devices, Station Q Copenhagen, Niels Bohr Institute, University of Copenhagen, Copenhagen 2100, Denmark*
[2]*Theoretische Physik, ETH Zürich, 8093 Zürich, Switzerland*
[3]*Nano-Science Center, Niels Bohr Institute, University of Copenhagen, Copenhagen 2100, Denmark*

(Received 5 February 2018; revised manuscript received 4 February 2019; published 21 February 2019)

We demonstrate the ability of an epitaxial semiconductor-superconductor nanowire to serve as a field-effect switch to tune a superconducting cavity. Two superconducting gatemon qubits are coupled to the cavity, which acts as a quantum bus. Using a gate voltage to control the superconducting switch yields up to a factor of 8 change in qubit-qubit coupling between the on and off states without detrimental effect on qubit coherence. High-bandwidth operation of the coupling switch on nanosecond time scales degrades qubit coherence.

DOI: 10.1103/PhysRevB.99.085434

I. INTRODUCTION

A significant challenge to scaling any quantum processor architecture is controlling interactions between qubits for multiqubit operations. Couplings between superconducting qubits are commonly controlled by detuning their transition frequencies [1,2]. In this way, instead of changing the qubit-qubit coupling constant, the effective coupling can be suppressed by making the qubit energies nondegenerate [3]. As superconducting qubits scale to larger networks, however, the increasingly crowded spectrum of qubit transition frequencies will make this approach prohibitively difficult. Increased frequency crowding makes residual couplings harder to suppress. Moreover, rearranging qubit frequencies, as is likely required during multiqubit operations, can lead to state leakage, as described by Landau-Zener physics [4–7]. For reasonable device parameters this results in leakage of several percent [8]. On-chip switchable coupling is desirable, since there is a tradeoff between fast two qubit gates and avoiding state leakage.

Tunable coupling schemes have been realized for nearest-neighbor-coupled flux-tunable qubits [9,10], as well as fixed frequency qubits [11]. These schemes allow qubits to be isolated for certain operations, for instance frequency retuning or single qubit rotations, while still enabling fast two qubit gates. A tunable superconducting microwave resonator has also been proposed for selective qubit coupling [12]. Such an approach has the advantage that a superconducting resonator, acting as a quantum bus, can mediate long-range interactions between superconducting qubits, and also allows increased connectivity between qubits [1,3,13,14]. Experimentally, flux control of resonators has been demonstrated [15,16] and used to couple superconducting qubits to spin ensembles [17].

While superconducting qubit circuits often use on-chip current lines to generate fluxes for control, the recently introduced gatemon superconducting qubit [18,19] is based on a voltage tunable semiconductor Josephson junction (JJ). Gatemons therefore allow for operation using voltages, which can be readily screened to minimize crosstalk and are compatible with semiconductor-based cryogenic control logic [20–22]. The advantage of voltage-controlled operation of semiconductor JJs suggests wider applications in a variety of superconducting circuits, such as superconducting field effect transistors (SFETs) [23].

Here, we implement a voltage controllable superconducting resonator—a tunable quantum bus—which is strongly coupled to two gatemon qubits. The bus is terminated by an SFET acting as a switch that allows *in situ* control of the resonator frequency and qubit-resonator coupling. We demonstrate that the coupling between the two gatemons can be switched between "on" and "off" states by controlling the SFET with on/off coupling ratios up to ∼8. We also show that when the coupling is turned off, the frequency of one qubit can be tuned through the other with a strong suppression of state leakage. Finally, we investigate switching the tunable bus on nanosecond time scales. Pulsing the coupler has a similar signature to exciting the qubits albeit with suppressed phase coherence. The underlying mechanism behind this observation remains unclear.

II. BACKGROUND

A schematic of the device is shown in Fig. 1(a). Both qubits $Q1$ and $Q2$ are capacitively coupled to a $\lambda/2$ bus resonator with coupling strengths $g_{1(2)} \propto e\beta V_{\mathrm{rms},1(2)}/\hbar$, where β is the ratio of coupling capacitance to total qubit capacitance, and $V_{\mathrm{rms},1(2)}$ is the root-mean-square of the zero-point voltage fluctuations of the resonator at the location of $Q1(2)$ [13]. With the qubits at the same frequency f_{Q1}, $f_{\mathrm{Q2}} = f_{\mathrm{Q}}$, detuned by $\Delta = 2\pi(f_{\mathrm{res}} - f_{\mathrm{Q}})$ from the resonator frequency f_{res}, the bus-mediated qubit-qubit coupling $g_{12} = g_1 g_2/\Delta$ [24,25] can be controlled by changing either Δ or $g_1 g_2$.

An open switch gives a voltage antinode at the qubit end of the resonator [blue in Fig. 1(a)], which results in a large $V_{\mathrm{rms},1(2)}$ with the resonator frequency given by the $\lambda/2$ mode, $f_{\mathrm{res}} = f_{\lambda/2}$. With the SFET in this open state, and f_{Q1}, f_{Q2} close to $f_{\lambda/2}$ we expect that the cavity-mediated coupling is turned on. On the other hand, when the switch is closed, a

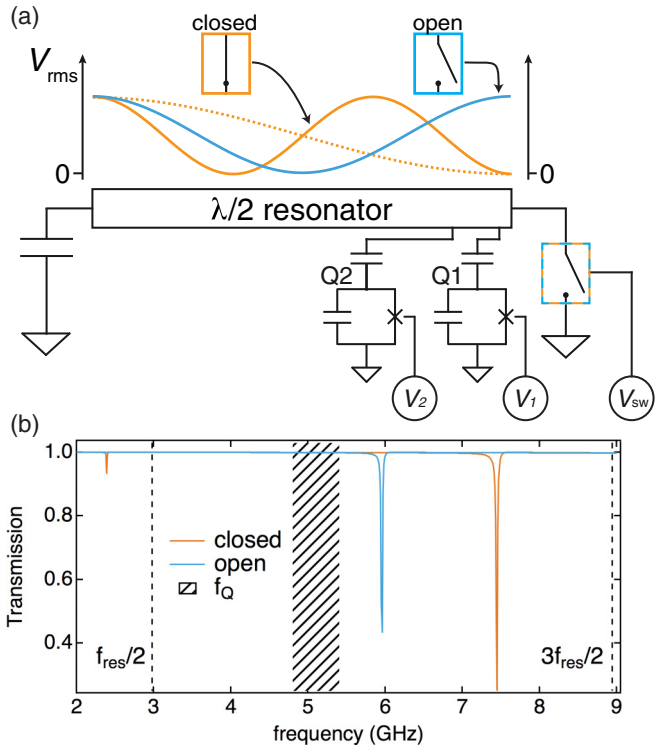

FIG. 1. Schematic and simulation of the voltage-controlled superconducting quantum bus. (a) Two gatemon qubits are capacitively coupled to a $\lambda/2$ resonator. One end of the resonator can be grounded through a voltage-controlled superconducting switch. Depending on the switch position being open (blue) or closed (orange), the rms voltage along the resonator length is changed, modifying the coupling between qubits by effectively turning the $\lambda/2$ resonator (blue) into a $\lambda/4$ resonator (orange). The dashed and solid orange lines represent the first and second modes of the $\lambda/4$ resonator respectively. (b) Simulated transmission through the feedline coupled to the tunable bus with the superconducting switch either open (blue) or closed (orange), supporting a large critical current (∼250 nA). The dashed shaded region indicates the range for the operating frequency of the qubits, f_Q.

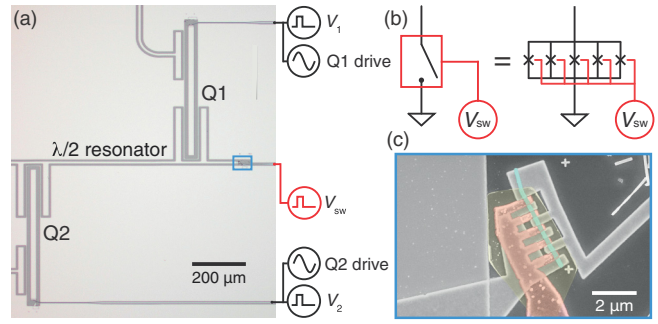

FIG. 2. Two-qubit device with switchable quantum bus. (a) Optical micrograph of the two-gatemon device with the $\lambda/2$ bus resonator terminated by a superconducting switch. Each qubit consists of a bar-shaped island and a gated Al-InAs-Al Josephson junction. (b) The superconducting switch consists of five parallel gated semiconducting weak link Josephson junctions controlled by a single gate voltage. (c) Scanning electron micrograph of the five top gated Al-InAs-Al Josephson junctions.

voltage node is enforced at the qubit end of the resonator, with its fundamental mode changing from $\lambda/2$ to $\lambda/4$. This turns off the interqubit coupling by reducing $V_{\mathrm{rms},1(2)}$ and moving the lowest bus modes to $f_{\lambda/2}/2$ and $3f_{\lambda/2}/2$, which are far detuned from the qubit frequencies [12].

We model the tunable bus as a transmission line terminated with an inductive load, given by the Josephson inductance $L_J = \frac{\hbar}{2eI_c}$. The bus is capacitively coupled to a feedline and we calculate the feedline transmission as a function of frequency [Fig. 1(b)]. With the switch in the open state [blue in Fig. 1(b)], no current flows in the SFET and we find $f_{\mathrm{res}} \sim 6$ GHz for the bare resonator, close to the typical qubit frequencies [dashed shaded region in Fig. 1(b)]. From transport measurements using similar semiconductor JJs, we estimate that the SFET in the closed state has a critical current $I_{\mathrm{c,closed}} \sim 250$ nA, corresponding to $L_J \sim 1$ nH (the SFET has five JJs connected in parallel, as discussed in Sec. III). As expected, the simulation shows two resonances [orange in Fig. 1(b)] at frequencies approaching $f_{\mathrm{res}}/2$ and $3f_{\mathrm{res}}/2$ [dashed black lines in Fig. 1(b)]. Using capacitance simulations we designed the qubit-bus coupling to be $g/2\pi \sim 80$ MHz for both qubits. With the switch in the open state and $\Delta/2\pi \sim 500$ MHz, this results in $g_{12}/2\pi \sim 13$ MHz. In the case where the switch is closed, the suppression of the coupling is determined by both the larger frequency detuning and reduction in $V_{\mathrm{rms},1(2)}$ of the bus modes. We estimate this residual coupling by applying the "black box" quantization formalism [26] and find that typical values for f_Q and $I_{\mathrm{c,closed}} \sim 250$ nA result in $g_{12}/2\pi \sim 1$ MHz. As the higher and lower bus modes contribute to $g_{12}/2\pi$ with opposite sign [27], we anticipate this residual coupling could be further suppressed by tuning the circuit such that the two contributions cancel. The direct capacitive coupling between the qubits is estimated to be <1 MHz.

III. EXPERIMENTAL REALIZATION AND MEASUREMENT TECHNIQUES

Figure 2(a) shows an optical image of the tunable bus device. The JJs for both the cavity and the qubits are superconductor-semiconductor-superconductor (S-Sm-S) junctions with a few-channel Sm region [28], allowing the Josephson coupling energy E_J to be tuned using a gate voltage that controls the carrier density in the Sm region. The two transmon-type gatemon qubits each consist of a bar-shaped island with a single JJ to ground. The SFET at the end of the tunable bus is made from several gate tunable JJs in parallel [Fig. 2(b)].

The device was fabricated following the recipe described in Ref. [29] and Appendix A. Both the qubits and the tunable bus JJs were formed by selectively wet etching a segment of a ∼30-nm-thick Al shell that was epitaxially grown around a ∼75-nm-diameter single-crystal InAs nanowire [30]. E_C/h of $Q1(2)$ was designed to be ∼200 MHz with E_J/E_C tuned to 75–90 using the side gate voltage $V_{1(2)}$. To reduce the effective inductance of the bus switch when closed, five parallel JJs were used to form the SFET. As shown in Fig. 2(c), the five junctions were etched into a single wire (blue) and then

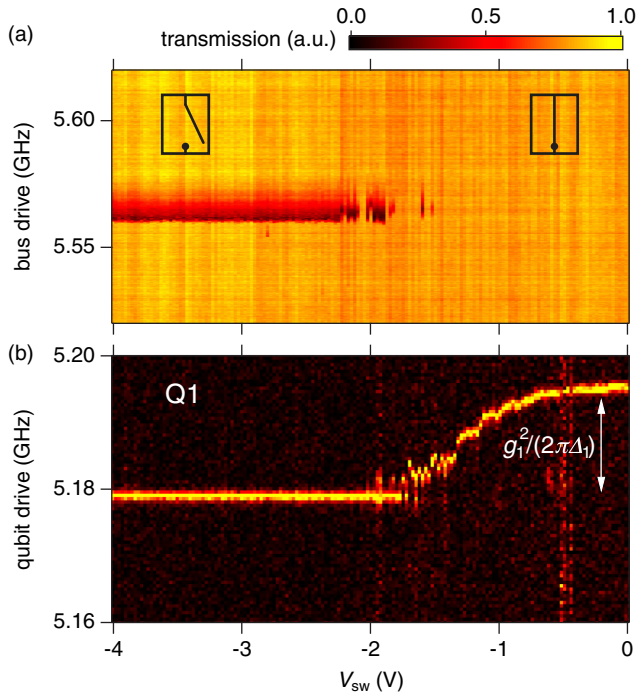

FIG. 3. Switchable bus and qubit spectroscopy. (a) Normalized transmission as a function of bus drive frequency and V_{sw}. (b) $Q1$ resonance frequency as a function of V_{sw}. The $Q1$ readout resonator response was measured while a qubit microwave drive tone probed the $Q1$ transition frequency.

covered with 15 nm of ZrO_2 dielectric (yellow) deposited by atomic layer deposition. The SFET was controlled with a common top gate voltage V_{sw} (red).

The qubits were manipulated using phase-controlled microwave pulses for rotations around axes in the X-Y plane of the Bloch sphere and voltage pulses on $V_{1,2}$ for rotations around the Z axis and fast frequency displacement [31]. Both X-Y and Z control pulses were applied through each qubit's gate line. Measured lifetimes and inhomogeneous dephasing times of the two qubits were ~4 μs and ~1-2 μs respectively, for the bus in both the on and off states. The two qubits were coupled to individual $\lambda/4$ superconducting cavities (with resonant frequencies $f_{C1} \sim 6.87$ GHz and $f_{C2} \sim 6.80$ GHz). These were then coupled to a common feedline for dispersive readout [32] with a superconducting traveling-wave parametric amplifier used to improve the signal-to-noise ratio [33]. The tunable bus was also coupled to the common feedline allowing an independent measurement of its resonance. The sample was placed inside an Al box, surrounded by a cryoperm shield and mounted at the mixing chamber of a cryogen-free dilution refrigerator with base temperature ~20 mK (see Appendix B).

IV. RESULTS AND DISCUSSIONS

Figure 3(a) shows vector network analyzer measurements of the tunable bus resonance as a function of V_{sw}. At large negative V_{sw}, a resonance is observed at $f_{\lambda/2} \sim 5.6$ GHz, which shows a quality factor $Q \sim 2000$, likely limited by internal losses and coupling to a dissipative environment via the SFET gate line. We anticipate that on-chip filtering of the gate line could increase the quality factor of the tunable bus [34]. While the Purcell effect could impose an upper bound on qubit lifetimes [35], for the qubits here with $T_1 \sim 4$ μs and detunings of several hundred MHz this is not a constraint. We attribute the asymmetry in the resonance line shape to impedance mismatch of the feedline input and output [36]. Going to more positive V_{sw}, the bus resonance disappears with some reentrant features indicating a nonmonotonic turn on of the SFET. We speculate that the disappearance of the resonance is due to the measurement excitation populating the bus with photons and thus driving the SFET normal, leading to a highly reduced Q factor. Although affecting our ability to directly track the bus frequency, it should not impact its role as a quantum bus for $Q1$ and $Q2$ as the coupling is mediated through virtual photons [24]. Interaction between the bus and the qubits renormalizes the qubit frequencies, allowing changes in the bus to be indirectly probed by measuring one of the qubits [Fig. 3(b)]. The push on f_{Q1} by the bus is given by the Lamb shift $\chi_1 = g_1^2/(\Delta_1)$ (white arrow), where $\Delta_1 = 2\pi(f_{res} - f_{Q1})$. When the SFET is depleted, the qubit frequency is pushed by the resonator with $f_{\lambda/2} \sim 5.6$ GHz. While closing the switch f_{Q1} increased, indicating that either the bus mode is moving up in frequency or g_1 is decreased, or both. We observed a crossing of the readout resonator with the bus resonator at around $V_{sw} = -0.5$ V, characterized by a stripe in the spectroscopy data where the readout visibility is reduced. Both the continuous change of the qubit frequency and the crossing of a resonance with the readout resonator indicate that the first mode of the $\lambda/2$ resonator (switch open) turns continuously into the second mode of the $\lambda/4$ resonator (switch closed). For $V_{sw} > -0.5$ V, the qubit frequency is roughly constant, indicating that either f_{res} no longer changes, or that g_1 is suppressed, although we cannot distinguish between these two effects.

Next, we turn to qubit coupling at fixed values of V_{sw} where the coupler is either on or off. We measured the spectrum while tuning $Q2$ into resonance with $Q1$ [Figs. 4(a) and 4(b)]. On resonance, the two-qubit states hybridize due to the bus-mediated coupling. As Fig. 4(a) illustrates, the splitting was small, although clearly nonzero, when the switch is closed. For an open switch the qubit coupling significantly increased, resulting in a larger splitting between hybridized states [Fig. 4(b)].

To further investigate the interqubit coupling, we performed experiments in the time domain. The two qubits were detuned by ~400 MHz and $Q1$ ($Q2$) was prepared in $|1\rangle$ ($|0\rangle$). A gate pulse was applied for a time τ to bring $Q2$ into resonance with $Q1$ [Fig. 4(c)]. Depending on τ and the pulse amplitude ΔV_2 elementary excitations swap between the two qubits. Figure 4(d) shows the swap oscillations with the coupler off and from sine fits to the oscillations, an interaction rate $g_{12}^{off}/2\pi \sim 3.2$ MHz is extracted, consistent with the avoided crossing measured in spectroscopy. With the coupler on, we observed significantly faster swap oscillations [Fig. 4(e)] and extract $g_{12}^{on}/2\pi \sim 18$ MHz.

Figure 4(f) plots the gatemon coupling strength extracted from swap oscillations as a function of qubit frequency. As expected, g_{12}^{on} (blue) depended strongly on the detuning from the bus. Assuming $g_1 = g_2 = g$ and fitting the data to $g_{12}^{on} =$

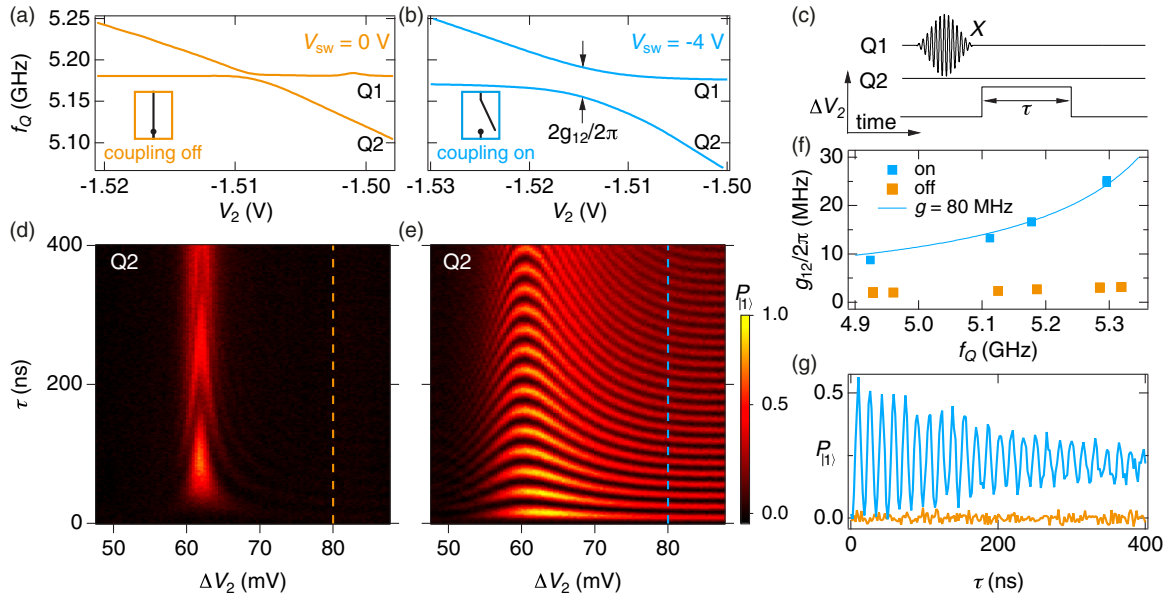

FIG. 4. Tunable coherent gatemon coupling. (a),[(b)] Measurement of the avoided level crossing between $Q1$ and $Q2$ for the switch closed (open), corresponding to gatemon coupling off (on) as a function of the qubit drive and V_2. (c) Pulse sequence to probe the coherent coupling between the qubits. With $Q1$ and $Q2$ detuned, $Q1$ is prepared in $|1\rangle$ and $Q2$ in $|0\rangle$. A square gate pulse with amplitude ΔV_2 is turned on for a time τ and brings $Q2$ close to or in resonance with $Q1$. (d),[(e)] The $|1\rangle$ state probability, $P_{|1\rangle}$, for $Q2$ as a function of ΔV_2 and τ for qubit coupling off (on). (f) Extracted gatemon coupling strengths for on and off case as a function of qubit resonance frequency. The solid line is a fit to the function $g_{12}^{\rm on} = g^2/\Delta$. (g) Cuts along the dashed lines in (d) and (e) at $\Delta V_2 = 80$ mV.

g^2/Δ yields $g/2\pi \sim 80$ MHz. We measured a residual off state coupling $g_{12}^{\rm off}/2\pi \sim 2$–$4$ MHz, limiting the maximum on/off coupling ratio observed in this experiment to $\sim$8. While a larger than anticipated L_J (due to a smaller $I_{c,\rm closed}$) might explain the residual coupling, our model gives an upper bound of $\sim$1 MHz for this coupling after accounting for the observation that the higher bus mode crosses the $Q1$ readout resonator. The dominant contributor to this residual coupling might then be spurious chip modes. Such modes could be suppressed through more careful microwave engineering, for example, by using air bridges [37].

Figure 4(g) shows cuts from Figs. 4(d) and 4(e) where the $Q1$ frequency crossed through the $Q2$ frequency and then back with the coupler either on or off. These data illustrate that even a modest switching ratio $g_{12}^{\rm on}/g_{12}^{\rm off} \sim 6$ allows both strong suppression of state leakage when the coupler is off and fast swaps when on. For a double passage Landau-Zener-Stückelberg process [8], a maximum state leakage of $\sim$50% in the on state (blue) indicates a level velocity of $\sim$80 MHz/ns [38]. Since the level velocity is the same for both coupler states, one can estimate a maximum state leakage of $\sim$2% in the coupler off state, comparable to the measurement noise here.

Finally, we investigated dynamic operation of the switch by pulsing $V_{\rm sw}$. Figure 5(a) shows the change of the qubit frequency f_{Q1} while controlling the bus. Again, f_{Q1} is pushed down at large negative $V_{\rm sw}$ due to the Lamb shift. We probed the effect that a fast voltage pulse on the switch has on $Q1$ through a Ramsey experiment. Two $X/2$ pulses were interleaved with a voltage pulse of the SFET gate [Fig. 5(b)]. The Ramsey experiment is sensitive to the Lamb shift induced qubit frequency change. Sitting at a dc offset $V_{\rm sw}^0 = -0.4$ V, for $\Delta V_{\rm sw} > 0$ V the Ramsey fringes remained roughly constant, as f_{Q1} does not change [Fig. 5(c)]. At high pulse amplitudes the visibility of the fringes was reduced, indicating reduced qubit coherence. We speculate that above certain amplitudes charge traps in the gate dielectric are excited and only relax on time scales comparable to the Ramsey experiment, causing decoherence, though further experiments would be needed to verify this.

While applying negative pulses ($\Delta V_{\rm sw} < 0$ V) to change the qubit coupling on a fast time scale, f_{Q1} was lowered, reducing the period of the Ramsey fringes. For the negative pulses above a certain critical amplitude, $\Delta V_{\rm sw}^{\rm c} \sim -1.1$ V,

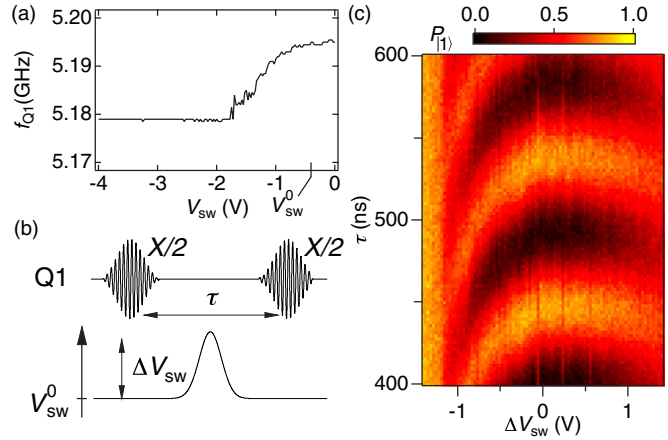

FIG. 5. Fast switch response. (a) Resonance frequency of $Q1$ as a function of $V_{\rm sw}$, extracted from Fig. 3(b). (b) Ramsey pulse sequence to probe the fast response of the switch inserting a fast Gaussian switch pulse ($\sigma = 64$ ns) with amplitude $\Delta V_{\rm sw}$ between two Ramsey pulses. (c) $P_{|1\rangle}$ as a function of $\Delta V_{\rm sw}$ and delay τ.

the readout response suggests that $Q1$ is excited into the $|1\rangle$ state and phase coherence is lost. The origin of this effect is presently unclear. We find that the value of $\Delta V_{\mathrm{sw}}^{\mathrm{c}}$ depends on both V_{sw}^{0} and the shape of the switch pulse. It was observed that the time scale on which the qubit can be coherently manipulated after a switch pulse is somewhat shorter than the decay time of the qubit, possibly indicating a different mechanism than qubit excitation like impairment of the readout resonator. Similar effects have been observed in two other samples: one device identical to that presented here, and the other using a $\lambda/4$ switchable resonator as the quantum bus. We speculate that pulsing the SFET close to depletion nonadiabatically excites the qubit circuit [39]. Another possibility is that pulsing the SFET JJs towards depletion generates quasiparticles that induce decoherence [40].

V. CONCLUSIONS

In summary, we have demonstrated a voltage-tunable superconducting quantum bus that can control the coherent coupling between two gatemons. The number of qubit pairs coupled through the tunable resonator could readily be increased, allowing for larger connectivity. This could be of interest for qubit architectures beyond the surface code geometry [41]. The continuously tunable coupling might also prove attractive for quantum simulation [42]. While dynamic operation of this voltage-controlled bus remains an outstanding problem, the potential advantages of this approach for coupling qubits motivates further investigations. Moreover, recent work integrating low loss microwave circuits with proximitized two-dimensional electron gases that support a wide range of critical currents provides an ideal platform to explore such voltage-controlled coupling schemes [43].

ACKNOWLEDGMENTS

We acknowledge helpful discussions with S. Nigg and V. Shumeiko. This work was supported by Microsoft Project Q, the U.S. Army Research Office, and the Danish National Research Foundation. N.J.P. acknowledges support from the Swiss National Science Foundation and NCCR QSIT. F.K. acknowledges support from the Danish Innovation Fund and C.M.M. acknowledges support from the Villum Foundation. The traveling-wave parametric amplifier used in this experiment was provided by MIT Lincoln Laboratory and Irfan Siddiqi Quantum Consulting (ISQC), LLC, via sponsorship from the U.S. Government.

APPENDIX A: SAMPLE FABRICATION

The sample is fabricated from a ∼100-nm-thick Al film on a high resistivity Si substrate. First the feed and control lines, gatemon islands, and readout resonators as well as windows for placing the nanowires (20 μm by 40 μm) are wet etched. Subsequently, molecular-beam epitaxy-grown nanowires are transferred from the growth chip to the etched windows using a dry deposition technique. A ∼200-nm segment of the Al shell is removed using a wet etch. The nanowire contacts are patterned from Al using a lift-off process with an ion mill step to remove the native Al_2O_3 prior to deposition. The tunable bus ZrO_2 gate dielectric is deposited using an atomic layer deposition lift-off process. Finally the qubit gates and the bus top gate are patterned from Al again using a lift-off process.

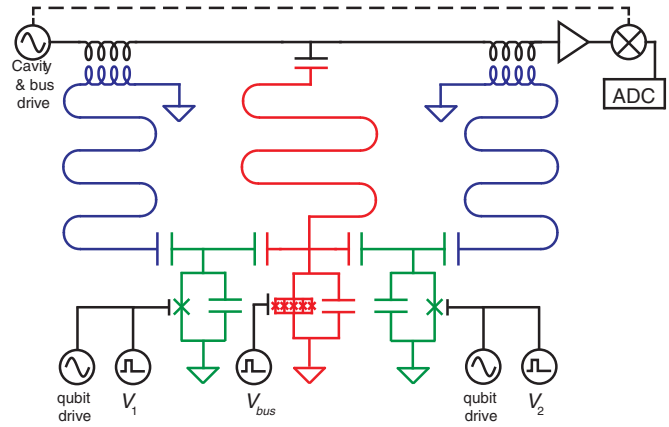

FIG. 6. Circuit diagram of the device, including readout resonators (blue), qubits (green), and the tunable bus (red).

APPENDIX B: MEASUREMENT SETUP

Figure 6 shows an electrical circuit diagram of the sample. All measurements presented in the paper are performed in a cryogen-free dilution refrigerator with a base temperature below 20 mK. The details of the fridge shielding as well as the line filtering are shown in Fig. 7. The sample is mounted inside an Al box to suppress magnetic fluctuations. This box is placed inside a Cu box used to mount the sample at the MC plate of the refrigerator. Both boxes are closed but not light tight; they are further surrounded by a cylindrical cryoperm shield, which is also thermally anchored to the mixing chamber.

To manipulate an individual qubit, a coaxial line and a dc line are used (green in Fig. 7). In contrast to earlier experiments, we use one single coax for both XY microwave control and fast gate voltage Z control as illustrated in Fig. 6. The coax line is filtered at high frequencies (>300 MHz) by a Minicircuits VLF-320 low-pass filter and an ECCOSORB filter. A key feature of the Minicircuits filter is the increased transmission at typical qubit resonance frequencies. The dc line is added with a bias tee at low temperature. The tunable bus is controlled with a coaxial and dc line as well (red). Since there is no need for microwave control, the low-pass filter used (Minicircuits VLFX-300) filters high frequencies much more efficiently. For readout (blue), a signal line is used, which is heavily attenuated (60 dB) to reduce both the thermal occupation of the resonator and noise to the sample. The readout line with magnetically shielded isolators allows signal out while suppressing any noise from the traveling-wave parametric amplifier (TWPA) and the cryogenic HEMT amplifier at the 4-K stage. The TWPA is driven with a microwave pump tone at ∼8 GHz [33] and shielded by a separate cryoperm shield. We note that the scheme in Fig. 7 only displays the setup for one qubit. For two qubit operation the green components have to be doubled.

The data in all figures in the main text were acquired using parallel heterodyne detection in the dispersive regime. On the signal line we combine two drives with frequencies close to

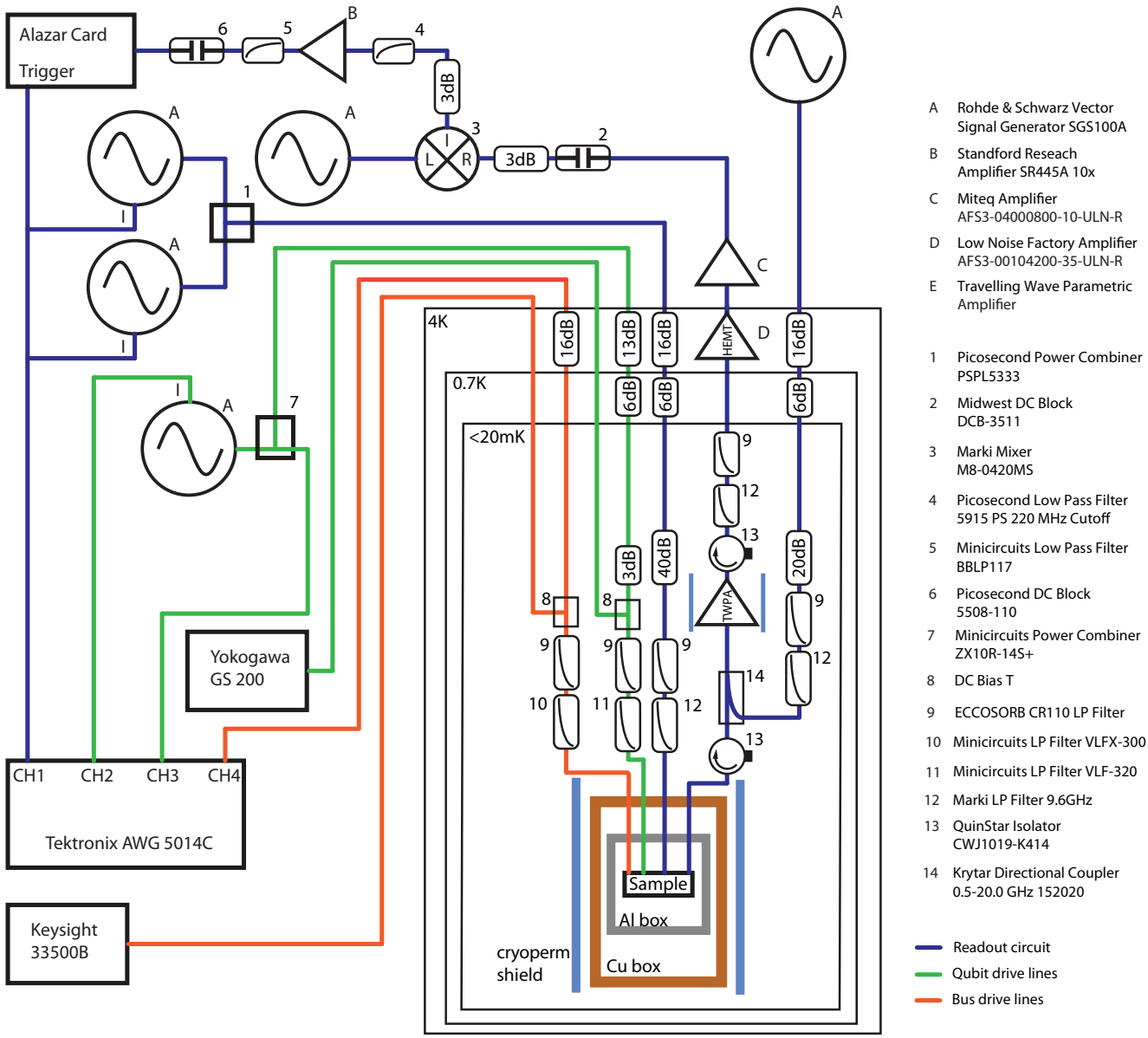

FIG. 7. Schematic of the experimental setup for readout of two qubits but manipulation of only one qubit.

the resonance frequencies of cavity 1 and cavity 2 (blue). After passing through the TWPA and HEMT amplifiers and another amplification step at room temperature the combined signal is mixed down to two intermediate frequencies with a local oscillator, before sampling and performing digital homodyne detection to extract the cavity magnitude response. Due to the low fidelity readout, qubit state measurements are obtained by averaging over many experimental runs. Qubit state assignments are calibrated using Rabi oscillations between the $|0\rangle$ and $|1\rangle$ states.

[1] L. DiCarlo, J. M. Chow, J. M. Gambetta, L. S. Bishop, B. R. Johnson, D. I. Schuster, J. Majer, A. Blais, L. Frunzio, S. M. Girvin, and R. J. Schoelkopf, Nature (London) **460**, 240 (2009).
[2] J. Kelly, R. Barends, B. Campbell, Y. Chen, Z. Chen, B. Chiaro, A. Dunsworth, A. G. Fowler, I.-C. Hoi, E. Jeffrey, A. Megrant, J. Mutus, C. Neill, P. J. J. O'Malley, C. Quintana, P. Roushan, D. Sank, A. Vainsencher, J. Wenner, T. C. White *et al.*, Phys. Rev. Lett. **112**, 240504 (2014).
[3] J. Majer, J. Chow, J. Gambetta, J. Koch, B. Johnson, J. Schreier, L. Frunzio, D. Schuster, A. A. Houck, A. Wallraff, A. Blais, M. Devoret, S. Girvin, and R. Schoelkopf, Nature (London) **449**, 443 (2007).
[4] L. Landau, Phys. Z. Sowjetunion **2**, 46 (1932).
[5] C. Zener, Proc. R. Soc. London, Ser. A **137**, 696 (1932).
[6] E. C. G. Stückelberg, Helv. Phys. Acta **5**, 369 (1932).
[7] E. Majorana, Nuovo Cimento **9**, 43 (1932).

[8] C. M. Quintana, K. D. Petersson, L. W. McFaul, S. J. Srinivasan, A. A. Houck, and J. R. Petta, Phys. Rev. Lett. **110**, 173603 (2013).

[9] R. C. Bialczak, M. Ansmann, M. Hofheinz, M. Lenander, E. Lucero, M. Neeley, A. D. O'Connell, D. Sank, H. Wang, M. Weides, J. Wenner, T. Yamamoto, A. N. Cleland, and J. M. Martinis, Phys. Rev. Lett. **106**, 060501 (2011).

[10] Y. Chen, C. Neill, P. Roushan, N. Leung, M. Fang, R. Barends, J. Kelly, B. Campbell, Z. Chen, B. Chiaro, A. Dunsworth, E. Jeffrey, A. Megrant, J. Y. Mutus, P. J. J. O'Malley, C. M. Quintana, D. Sank, A. Vainsencher, J. Wenner, T. C. White *et al.*, Phys. Rev. Lett. **113**, 220502 (2014).

[11] D. C. McKay, S. Filipp, A. Mezzacapo, E. Magesan, J. M. Chow, and J. M. Gambetta, Phys. Rev. Appl. **6**, 064007 (2016).

[12] M. Wallquist, V. S. Shumeiko, and G. Wendin, Phys. Rev. B **74**, 224506 (2006).

[13] A. Wallraff, D. I. Schuster, A. Blais, L. Frunzio, R.-S. Huang, J. Majer, S. Kumar, S. M. Girvin, and R. J. Schoelkopf, Nature (London) **431**, 162 (2004).

[14] M. A. Sillanpää, J. I. Park, and R. W. Simmonds, Nature (London) **449**, 438 (2007).

[15] M. Sandberg, C. M. Wilson, F. Persson, T. Bauch, G. Johansson, V. Shumeiko, T. Duty, and P. Delsing, Appl. Phys. Lett. **92**, 203501 (2008).

[16] A. Palacios-Laloy, F. Nguyen, F. Mallet, P. Bertet, D. Vion, and D. Esteve, J. Low Temp. Phys. **151**, 1034 (2008).

[17] Y. Kubo, C. Grezes, A. Dewes, T. Umeda, J. Isoya, H. Sumiya, N. Morishita, H. Abe, S. Onoda, T. Ohshima, V. Jacques, A. Dréau, J.-F. Roch, I. Diniz, A. Auffeves, D. Vion, D. Esteve, and P. Bertet, Phys. Rev. Lett. **107**, 220501 (2011).

[18] G. de Lange, B. van Heck, A. Bruno, D. J. van Woerkom, A. Geresdi, S. R. Plissard, E. P. A. M. Bakkers, A. R. Akhmerov, and L. DiCarlo, Phys. Rev. Lett. **115**, 127002 (2015).

[19] T. W. Larsen, K. D. Petersson, F. Kuemmeth, T. S. Jespersen, P. Krogstrup, J. Nygard, and C. M. Marcus, Phys. Rev. Lett. **115**, 127001 (2015).

[20] D. R. Ward, D. E. Savage, M. G. Lagally, S. N. Coppersmith, and M. A. Eriksson, Appl. Phys. Lett. **102**, 213107 (2013).

[21] H. Al-Taie, L. W. Smith, B. Xu, P. See, J. P. Griffiths, H. E. Beere, G. A. C. Jones, D. A. Ritchie, M. J. Kelly, and C. G. Smith, Appl. Phys. Lett. **102**, 243102 (2013).

[22] J. M. Hornibrook, J. I. Colless, I. D. Conway Lamb, S. J. Pauka, H. Lu, A. C. Gossard, J. D. Watson, G. C. Gardner, S. Fallahi, M. J. Manfra, and D. J. Reilly, Phys. Rev. Appl. **3**, 024010 (2015).

[23] Z. Qi, H.-Y. Xie, J. Shabani, V. E. Manucharyan, A. Levchenko, and M. G. Vavilov, Phys. Rev. B **97**, 134518 (2018).

[24] A. Blais, R.-S. Huang, A. Wallraff, S. M. Girvin, and R. J. Schoelkopf, Phys. Rev. A **69**, 062320 (2004).

[25] A. Sørensen and K. Mølmer, Phys. Rev. Lett. **82**, 1971 (1999).

[26] S. E. Nigg, H. Paik, B. Vlastakis, G. Kirchmair, S. Shankar, L. Frunzio, M. H. Devoret, R. J. Schoelkopf, and S. M. Girvin, Phys. Rev. Lett. **108**, 240502 (2012).

[27] S. Filipp, M. Göppl, J. M. Fink, M. Baur, R. Bianchetti, L. Steffen, and A. Wallraff, Phys. Rev. A **83**, 063827 (2011).

[28] A. Kringhøj, L. Casparis, M. Hell, T. W. Larsen, F. Kuemmeth, M. Leijnse, K. Flensberg, P. Krogstrup, J. Nygård, K. D. Petersson, and C. M. Marcus, Phys. Rev. B **97**, 060508 (2018).

[29] L. Casparis, T. W. Larsen, M. S. Olsen, F. Kuemmeth, P. Krogstrup, J. Nygård, K. D. Petersson, and C. M. Marcus, Phys. Rev. Lett. **116**, 150505 (2016).

[30] P. Krogstrup, N. L. B. Ziino, W. Chang, S. M. Albrecht, M. H. Madsen, E. Johnson, J. Nygård, C. M. Marcus, and T. S. Jespersen, Nat. Mater. **14**, 400 (2015).

[31] Rotations $R_I(\theta) = e^{\pm i\sigma_I\theta/2}$ $(I = X, Y, Z)$ are abbreviated in the text with I for $\theta = \pi$ and $I/2$ for $\theta = \pi/2$.

[32] R. Barends, J. Kelly, A. Megrant, D. Sank, E. Jeffrey, Y. Chen, Y. Yin, B. Chiaro, J. Mutus, C. Neill, P. O'Malley, P. Roushan, J. Wenner, T. C. White, A. N. Cleland, and J. M. Martinis, Phys. Rev. Lett. **111**, 080502 (2013).

[33] C. Macklin, K. O'Brien, D. Hover, M. E. Schwartz, V. Bolkhovsky, X. Zhang, W. D. Oliver, and I. Siddiqi, Science **350**, 307 (2015).

[34] X. Mi, J. V. Cady, D. M. Zajac, J. Stehlik, L. F. Edge, and J. R. Petta, Appl. Phys. Lett. **110**, 043502 (2017).

[35] A. A. Houck, J. A. Schreier, B. R. Johnson, J. M. Chow, J. Koch, J. M. Gambetta, D. I. Schuster, L. Frunzio, M. H. Devoret, S. M. Girvin, and R. J. Schoelkopf, Phys. Rev. Lett. **101**, 080502 (2008).

[36] A. Megrant, C. Neill, R. Barends, B. Chiaro, Y. Chen, L. Feigl, J. Kelly, E. Lucero, M. Mariantoni, P. J. J. O'Malley, D. Sank, A. Vainsencher, J. Wenner, T. C. White, Y. Yin, J. Zhao, C. J. Palmstrøm, J. M. Martinis, and A. N. Cleland, Appl. Phys. Lett. **100**, 113510 (2012).

[37] Z. Chen, A. Megrant, J. Kelly, R. Barends, J. Bochmann, Y. Chen, B. Chiaro, A. Dunsworth, E. Jeffrey, J. Y. Mutus, P. J. J. O'Malley, C. Neill, P. Roushan, D. Sank, A. Vainsencher, J. Wenner, T. C. White, A. N. Cleland, and J. M. Martinis, Appl. Phys. Lett. **104**, 052602 (2014).

[38] The level velocity depends on the slope of the qubit spectrum and rise time of the pulse detuning the qubit. We note that for the data in Fig. 4, the $Q2$ spectrum approaches a maximum at higher pulse amplitudes, resulting in prolonged swap oscillations.

[39] Y.-P. Shim and C. Tahan, Nat. Commun. **7**, 11059 (2016).

[40] U. Patel, I. V. Pechenezhskiy, B. L. T. Plourde, M. G. Vavilov, and R. McDermott, Phys. Rev. B **96**, 220501 (2017).

[41] T. Jochym-O'Connor and S. D. Bartlett, Phys. Rev. A **93**, 022323 (2016).

[42] I. Buluta and F. Nori, Science **326**, 108 (2009).

[43] L. Casparis, M. R. Connolly, M. Kjaergaard, N. J. Pearson, A. Kringhøj, T. W. Larsen, F. Kuemmeth, T. Wang, C. Thomas, S. Gronin, G. C. Gardner, M. J. Manfra, C. M. Marcus, and K. D. Petersson, Nat. Nanotechnol. **13**, 915 (2018).